mmEar: Push the Limit of COTS mmWave Eavesdropping on Headphones

Xiangyu Xu[†], Yu Chen[†], Zhen Ling[†*], Li Lu[‡], Junzhou Luo[†] and Xinwen Fu[¶]
[†]Southeast University, China, Email: {xy-xu, yu-chen, zhenling, jluo}@seu.edu.cn
[‡]Zhejiang University, China, Email: li.lu@zju.edu.cn
[¶]University of Massachusetts Lowell, Lowell, MA, USA, Email: xinwen_fu@uml.edu

***Abstract*—Recent years have witnessed a surge of headphones (including in-ear headphones) usage in works and communications. Because of the privacy-preserve property, people feel comfortable having confidential communication wearing headphones and pay little attention to speech leakage. In this paper, we present an end-to-end eavesdropping system, *mmEar*, which shows the feasibility of launching an eavesdropping attack on headphones leveraging a commercial mmWave radar. Different from previous works that realize eavesdropping by sensing speech-induced vibrations with reasonable amplitude, *mmEar* focuses on capturing the extremely faint vibrations with a low signal-to-noise ratio (SNR) on the surface of headphones. Toward this end, we propose a faint vibration emphasis (FVE) method that models and amplifies the mmWave responses to speech-induced vibrations on the In-phase and Quadrature (IQ) plane, followed by a deep denoising network to further improve the SNR. To achieve practical eavesdropping on various headphones and setups, we propose a cGAN model with a pretrain-finetune scheme, boosting the generalization ability and robustness of the attack by generating high-quality synthesis data. We evaluate *mmEar* with extensive experiments on different headphones and earphones and find that most of them can be compromised by the proposed attack for speech recovery.**

***Index Terms*—side-channel attack, headphone eavesdropping, mmWave sensing**

I. Introduction

The global headphone market size (including in-ear headphones) is valued at more than 58 billion in 2022 and is expected to grow at a compound annual growth rate of 12.6% from 2023 to 2030[1], showing an unstoppable trend of increasing headphone usage in the daily lives for people around the world. Besides the usage of entertainment, nowadays more and more people choose to wear headphones for working, including phoning, attending online conferences, and listening to voice messages. Compared to other alternatives (e.g., loudspeakers), headphones limit the transmission of sound close to the human ear, greatly reducing sound leakage. In that case, headphone users usually pay little attention to the threats of eavesdropping, making room for potential side-channel attacks.

Several side-channel attacks on loudspeakers leveraging non-acoustic sensors have been revealed by previous studies. The key insight is that when a loudspeaker generates sound waves, it induces the physical vibration of itself and the surrounding objects. Instead of directly recording the sound, side-channel eavesdropping attacks focus on capturing the sound-induced vibrations. Optical sensors, including lasers[2], high-speed cameras[3], electro-optical sensors[4] and lidars[5] could capture the vibrations for voice eavesdropping, under the assumption of static targets and no occlusion. With the surge of mobile devices, the built-in motion sensors are exploited to infer the speech[6], [7], [8], [9], [10], under the assumption of accessible motion sensor data. More recently, radio frequency (RF), such as Wi-Fi[11], [12] and UWB[13], has been explored for contactless eavesdropping, but not robust to noise. Due to their constraints, all these attacks could not yet threaten the headphone scenarios.

With the development of 5G and IoT, researchers find that mmWave signal could capture small vibrations[14] and thus enable eavesdropping on loudspeakers[15], sound wave-induced objects[16] and smartphones[17], [18]. These approaches work well with enough strength and signal-to-noise ratio (SNR) of the sound-induced vibrations. However, eavesdropping on headphones with mmWave signal is much more challenging as most sound-induced vibrations are wakened and absorbed within the headphone structure. To tackle this problem and enable headphone eavesdropping with a commercial-of-the-shelf (COTS) mmWave radar, we face the following challenges. First, the sound-induced vibrations on the headphone surface are too weak that a COTS mmWave radar could barely capture their pattern, and the SNR of captured sound-induced vibrations is too low that the noises dominate the influences on mmWave signals. Second, there are various headphones with different structures and materials, and the setups in real-world scenarios can also be different, making a versatile eavesdropping attack on different headphones and setups extremely difficult and costly.

In this work, we address the above challenges and propose *mmEar*, a practical mmWave-based headphone eavesdropping scheme using single COTS mmWave radar. To capture the faint speech-induced vibrations on the headphone surface, we propose a faint vibration emphasis (FVE) method that amplifies the vibration-induced phase changes of reflected mmWave signal on the In-phase and Quadrature (IQ) plane, followed by a deep denoising network to further improve the SNR of the captured sound-induced vibrations, so that the sound information carried by the vibrations could be partially revealed from the mmWave signals. To further improve the quality and intelligibility of the extracted sound information, we propose a cGAN model with a pretrain-finetune scheme, which leverages the physical mechanism of vibration generation on headphones

[*] Corresponding author: Prof. Zhen Ling of Southeast University, China.

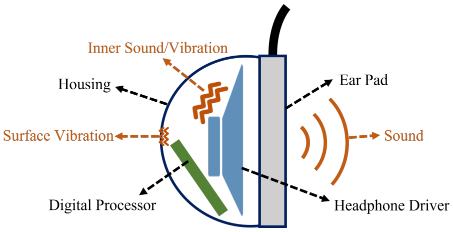

Fig. 1: A typical headphone structure and related sound/vibrations.

to generate large-amount synthesis pretraining data for various headphones and setups, followed by a finetune step with small amount real-world collected data to strengthen the robustness of the model, and finally recover the speech on the headphone and accomplish the eavesdropping. Overall, our contributions are summarized as follows:

- Our work reveals a practical non-contact eavesdropping attack on headphones leveraging single COTS mmWave radar, which demonstrates the alarming threat of user privacy leakage from widely used headphones.
- We propose FVE, a method for capturing faint speech-induced vibrations with low SNR from mmWave signals, which improves the perceived granularity for mmWave radars and extends their eavesdropping scenarios.
- We design a cGAN model with a dedicated pretrain-finetune scheme and a synthesis data generation approach to ensure that our attack could recover intelligible speech from different headphones and various setups with a small amount of real-world collected data.
- We performed extensive experiments to evaluate the proposed attack on different headphones and setups, demonstrating that most of them can be compromised by the proposed attack for speech recovery.

II. Background and Threat Model

A. Headphone Vibration

Fig. 1 depicts the typical structure of a headphone and the related sound/vibrations when playing an audio signal. The sound wave is generated from the driver and most signals propagate through the ear pad to human ears, providing high-quality sound to users. Meanwhile, there are some sound signals and sound-induced vibration signals within the headphone. Part of these signals transmits to the housing part of the headset, suffering great attenuation, and finally inducing faint vibrations on the surface of the headphone. With a normal sound volume setup, such pulses are too tiny to be observed.

B. mmWave FMCW Radar

The Frequency-Modulated Continuous Waveform (FMCW) mmWave radar works by transmitting chirp signals whose frequency increases linearly over time. Then the radar collects signals reflected from reflectors and mixes the received signal with the transmitting signal to generate the intermediate frequency (IF) signal, whose frequency is proportional to the time the chirp signal travels. Thus, the distance between the radar and reflectors could be measured from the IF signal given a fixed mmWave signal transmission speed.

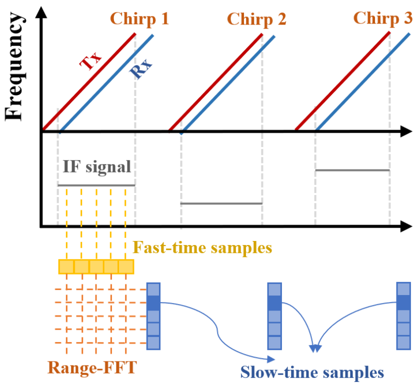

Fig. 2: Range-FFT on fast-time samples is needed to locate the target bin and phase variations of slow-time samples is used to capture the tiny displacement.

In practice, to measure the distance, a Fast Fourier Transform (i.e., range-FFT) is applied. As shown in Fig. 2, for each transmitting and receiving chirp pair, range-FFT generates a series of fast-time samples referred to as range bins, each corresponding to a discretized distance. For a COTS mmWave radar with $4GHz$ bandwidth for FMCW chirps, the distance measurement resolution is around $3.75cm$, which could generally locate the target (such as a headphone), but far from capturing the faint speech-induced vibrations.

For more fine-grained vibration sensing, the phase variations of the IF signal from the target range bin are needed. As depicted in Fig. 2, the samples in every chirp in a target range bin form the slow-time samples, and the phase variation caused by displacement changes Δd could be measured from the slow-time samples as $\Delta\phi = \frac{2\pi\Delta d}{\lambda}$, where λ denotes the wavelength of the mmWave chirp signal. Given the mm-level wavelength for mmWave radars, um-level displacement changes could be detected[17], which could capture the faint speech-induced vibrations from the headphones **if not considering the real-world noises**.

C. Threat Model

Scenarios: The scenario could be that a victim is making phone calls or participating in online conferences using headphones, which happens every day in the subway, café, etc. Meanwhile, an attacker co-located with the victim leverages a COTS mmWave radar sensor (which could be hidden in bags) to transmit mmWave signals toward the surface of the target headphones to perform eavesdropping. The goal of the attacker is to recover the speech content played in the headphone.

Assumptions: We assume that there are no physical blockages between the victim's headphones and the mmWave radar so that the mmWave signals can be transmitted directly toward the headphone of the victim. We do not assume the attacker installs any malware or attaches any customized hardware on the victim's device. And **we do not assume the adversary has prior knowledge of the victim's headphone type and the attack scenario context information**.

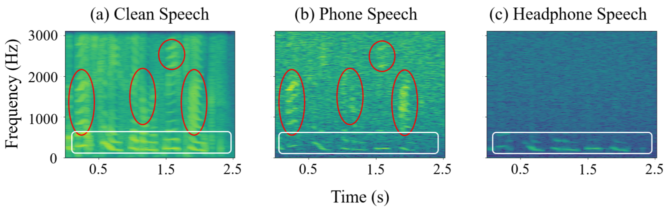

Fig. 3: The comparison between spectrogram of clean speech (a), speech recovered from the phone (b), and the speech captured from the headphone (c).

III. Feasible Study

We first explore the feasibility of capturing the patterns of speech-induced vibrations on the headphone surfaces in real-world scenarios. As described in Section. II, phase variations of the mmWave IF signal can be utilized for tiny vibration detection. Based on this principle, preliminary experiments were conducted with a COTS TI AWR1642 mmWave radar and an HP GH10GS headphone. The distance between the headphone and the mmWave radar is kept constant at $50cm$. During experiments, audio clips sourced from the "Harvard Sentences" in the Harvard Speech Corpus (HSC)[19] are played on the headphone. Meanwhile, the mmWave radar captures the speech-induced vibrations on the headphone surface as phase variations following the operations described in Section. II, and the extracted phase variations are then transformed into the corresponding spectrogram using Short-Time Fourier Transform (STFT).

For comparison, an iPhone 13 with earpiece mode on is tested under the same setup, since previous works[17], [18] have explored the feasibility of eavesdropping on smartphones' earpieces using mmWave radars. The results are shown in Fig. 3. The sound-induced vibrations from smartphones' earpieces could be roughly captured. While for headphones, due to the weaker vibration and lower SNR, most patterns are lost, leaving only limited and vague patterns on the spectrogram that could hardly represent the speech information.

To further improve the perceived granularity, we explore the phase variations of mmWave signals on vibration detection. Specifically, when plotting the phase variation samples on the In-phase and Quadrature (IQ) plane, theoretically, these samples could form arc-shape trajectories whose length is proportional to vibration amplitudes[20]. Considering the background noises, the arc trajectory could be shifted on the IQ plane and the linear relation between the arc length and the vibration amplitudes may not be kept. Fig. 4 illustrates the vibration-induced phase variations on the IQ plane. It can be seen that with relatively large vibration amplitudes and high SNR (such as vibrations on loudspeakers), the circle related to the arc trajectory could be fit and the linear relation could be regained by translating the circle center to the origin of IQ plane. On the other hand, with relatively small vibration amplitude and low SNR (such as vibrations on headphone surfaces), the sample trajectories lose the arc shape, making the circle fitting almost impossible, which prevents high-quality pattern capturing with mmWave signals. Although a recent work[21] proposes a multi-signal consolidation (MSC) model to guide the extraction of tiny machine vibrations, that could not help in extremely low SNR cases.

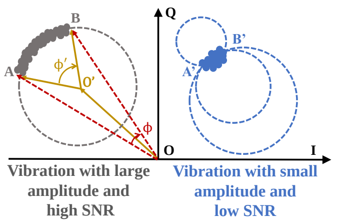
A
B
φ'
O'
φ
Q
B'
A'
O
I
Vibration with large amplitude and high SNR
Vibration with small amplitude and low SNR

Fig. 4: Phase variation fitting on the IQ plane.

According to our studies, **extremely faint sound-induced vibrations with low SNR have made eavesdropping on headphones a new challenging task for COTS mmWave radars**, necessitating the design of more refined signal processing approaches to capturing the speech patterns.

IV. System Overview

We design and implement a mmWave-based headphone eavesdropping system, *mmEar*. With the system, an attacker could leverage a COTS mmWave radar to capture the faint surface vibrations induced by the speech playing on the target headphone and recover the corresponding speech information, as the attack roadmap shown in Fig. 5. For constructing *mmEar*, the architecture contains two modules:

A. Headphone Speech-vibration Capturing Module

This module aims to extract the faint speech-induced vibrations on the surface of the headphone and enhance the corresponding speech patterns. After the basic mmWave signal processing procedure, *mmEar* determines the relative distance between the radar and the target headphone by range bin selection. Then, a faint vibration emphasis (FVE) approach is proposed to amplify the speech-induced vibrations aiming at improving their intelligibility, followed by a deep denoising network to enhance the corresponding speech patterns.

B. Headphone Eavesdropping Enhancement Module

To further improve the quality and intelligibility of the extracted speech signal on various headphones, *mmEar* designs a Conditional Generative Adversarial Network (cGAN) model[22] with a pretrain-finetune scheme. Concretely, following the physical mechanism of sound-induced vibration on headphones, a synthesis data generation method is proposed to stimulate mmWave responses for various headphones and setups, and form a large dataset for pretraining. Then a small amount of real-world data is collected to finetune the model, further improving the robustness of the attack.

V. Headphone Speech-vibration Capturing

A. Headphone Localization

To capture the speech-induced vibrations from the headphone surface, *mmEar* first localizes the target headphone, which involves a range-FFT to separate the space into multiple bins, each representing a different distance from the mmWave

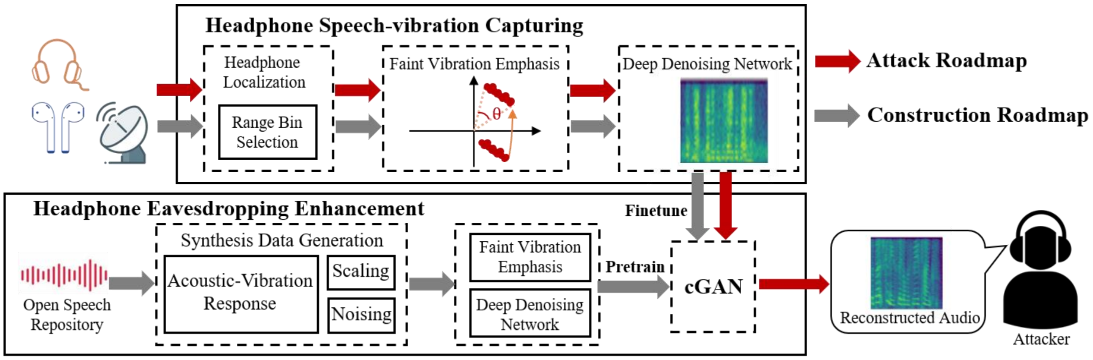

Fig. 5: Overview of mmEar architecture.

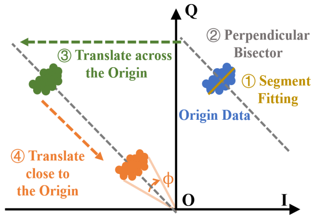
Q
② Perpendicular Bisector
③ Translate across the Origin
① Segment Fitting
Origin Data
④ Translate close to the Origin
ϕ
O
I

Fig. 6: Procedure of the FVE approach.

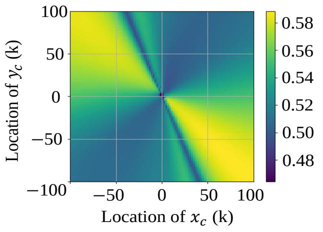

Fig. 7: STOI heatmap on the IQ plane.

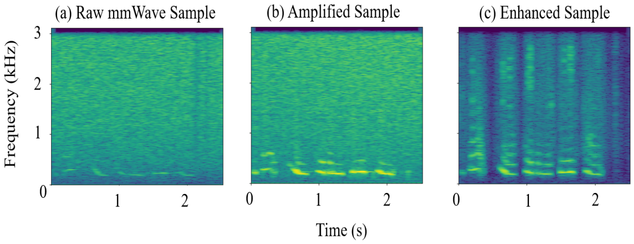

Fig. 8: Illustration of the FVE-amplified sample and network-enhanced sample.

radar. Therefore, the headphone localization problem becomes a range bin selection problem. Note from Fig. 3 that for the correct range bin, there are detectable low-frequency ($< 1000Hz$) patterns of phase variations on the spectrogram, which do not hold for other bins. Based on the observation, *mmEar* calculates the variance of phase variations for $1s$ within the frequency between $100Hz$ and $500Hz$ for each range bin and selects the largest one as the target.

B. Faint Vibration Emphasis

After range bin selection, the phase variations of the IF mmWave signal of the target range bin can be calculated to capture the vibrations. However, as discussed in Section.III, the sound-induced vibrations on headphones are too faint and with low SNR, making existing circle-fitting-based approaches[20][21] fail on the IQ plane.

To capture the faint headphone vibrations with low SNR, we propose a faint vibration emphasis (FVE) approach to amplify the phase variations on the IQ plane to improve intelligibility. As shown in Fig. 6, the procedure of FVE contains 4 steps:

- **Step 1:** Because of extremely small amplitude and low SNR, the phase variation trajectory looks more like a short thick line segment instead of an arc. Therefore, we fit the line segment leveraging the least square fitting.
- **Step 2:** Although we could not conduct circle-fitting because of the loss of arc shape for phase variation trajectories, given the fitted line segment obtained from Step 1, it could be observed that the center of the expected circle should lie on the perpendicular bisector of the line segment. So *mmEar* calculates the corresponding perpendicular bisector in this step.
- **Step 3:** In the circle-fitting process, the final step is to move the center of the fitted circle to the origin of the IQ plane. In our case, we got a line across the center of the circle from Step 2 instead. So we translate the line to make it across the origin of the IQ plane and move the phase variation trajectories accordingly.
- **Step 4:** Finally, to amplify the phase variations on the IQ plane, *mmEar* further translate the phase variation trajectories in Step 3 along with its perpendicular bisector toward the origin of the IQ plane, until the angle ϕ in Fig.6 reaches a pre-determined value Φ, which is set as $30°$ in *mmEar*. The impact of this value is evaluated in Section. VII-G.

To show the effectiveness of FVE, we calculate the short-term objective intelligibility (STOI)[23] when translating the phase variation trajectories in Fig. 6 to different coordinates on the IQ plane. The result is shown in Fig. 7. The higher value denotes better intelligibility. It can be observed from Fig. 6 and Fig. 7 that FVE does improve the intelligibility after translating the phase variation trajectories on the IQ plane. Fig. 8b further illustrates the spectrogram of the amplified vibration signal after FVE, compared to the raw spectrogram (Fig. 8a), the amplified spectrogram exhibits enhanced speech patterns, especially in low-frequency areas.

Note that a fitted line is always accessible for the phase variation trajectory. However, FVE could fail to improve the intelligibility when the vibration of the headphone body is too small to be captured by mmWave radar. Section VII-F discusses the scenario when the vibration is not large enough to be captured due to the small volume of headphones.

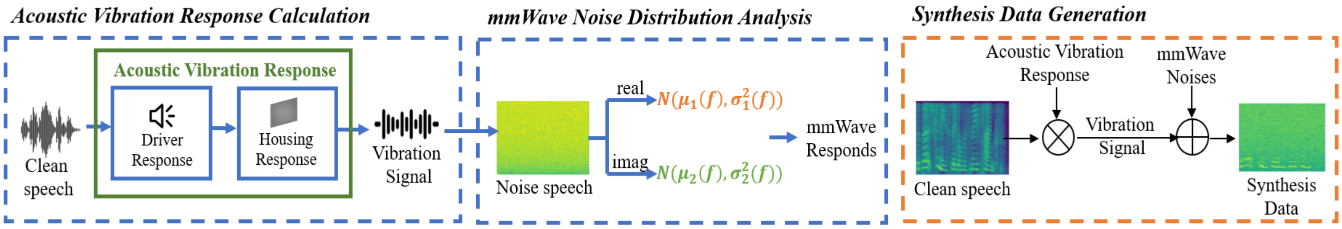
Acoustic Vibration Response Calculation
mmWave Noise Distribution Analysis
Synthesis Data Generation
Acoustic Vibration Response
Clean speech
Driver Response
Housing Response
Vibration Signal
Noise speech
real
$N(\mu_1(f), \sigma_1^2(f))$
imag
$N(\mu_2(f), \sigma_2^2(f))$
mmWave Responds
Acoustic Vibration Response
mmWave Noises
Vibration Signal
Clean speech
Synthesis Data

Fig. 9: The process of synthesis data generation in *mmEar*.

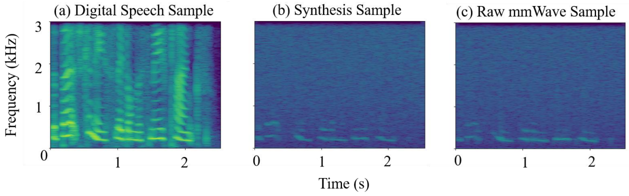

Fig. 10: Spectrograms of digital speech sample(a), synthesis sample (b) and mmWave-captured real-world sample (c).

C. Speech Pattern Enhancement

It could be observed from Fig. 8 that FVE significantly amplifies the speech patterns under $1000Hz$, but the speech patterns higher than $1000Hz$ are still buried in noise. To address the problem, we apply a deep denoising network model for speech pattern enhancement[24] to improve the SNR in the high-frequency range where a feed-forward neural network with many levels of non-linearities is adopted. The corresponding result is shown in Fig. 8c. We could observe that the speech-related pattern is enhanced in the high-frequency component after applying the model.

VI. Headphone Eavesdropping Enhancement

To further improve the intelligibility of the extracted speech signal, as well as extend the attack scope to various headphones and setups, *mmEar* designs a cGAN model[22] with a pretrain-finetune scheme to realize the headphone eavesdropping enhancement, which includes a synthesis data generation method and a cGAN enhancing process.

A. Synthesis Training Data Generation

The goal is to create a large amount of data that has similar signal patterns with real-world-collected mmWave samples when sensing the headphone vibrations. Moreover, the generated data should cover the influences of different headphones and setups. Toward this end, the process is presented in Fig. 9. We model the physical process from a digital speech sample to the mmWave responses by *acoustic vibration response calculation* and *mmWave noise distribution analysis*, and design the data generation procedure accordingly.

Acoustic-vibration Response Calculation. mmEar works by capturing the speech-induced vibrations on the headphone surface. Thus, to generate synthesis data, we first model the responses from digital acoustic signals to headphone vibrations in Fig. 9, It can be seen that digital speech signal is first influenced by the frequency response of the headphone drivers, generating physical acoustic signals. Then, the physical acoustic signals induce vibrations on the surface of smartphones, which is modulated by the acoustic-vibration transformation response of the headphone. Let f_d represent the frequency response function of a headphone driver, f_h denotes the acoustic-vibration transformation response of the headphone, and the frequency response function from digital speech to headphone vibrations could be modeled as $\alpha \cdot f_d \cdot f_h$, where α is the damping factor representing the signal attenuation.

Noise Distribution Analysis. From the speech-induced headphone vibrations, *mmWave* captures the vibration pattern for further speech recovery. To generate samples close to real-world mmWave data, we further analyze the distribution of mmWave noises. Specifically, we utilize mmWave radar to capture noises in the absence of any sound from the headphones. Then, STFT is employed to obtain the time-frequency spectrogram for mmWave noises. For each frequency component over time, the most commonly-used signal amplitude does not show any obvious pattern. And we further analyze the real and imaginary parts separately). Through the Kolmogorov-Smirnov test (K-S test)[25], [26], all p-values for each frequency component are found to be greater than 0.05, indicating that **the mmWave noise in each frequency component, both real and imaginary parts, follows an independent normal distribution, respectively**.

Systhesis Data Generation. With the model of acoustic-vibration responses and mmWave noises, the mmWave responses on speeches played on a headphone could be roughly modeled as:

$$S_{mm} = STFT(S_{raw}) \cdot \alpha \cdot f_d \cdot f_h + \beta \cdot (\delta_r + j \cdot \delta_i), \quad (1)$$

where $SFTF(\cdot)$ denotes the STFT operation, S_{raw} denotes the digital speech samples in HSC, α and β are factors denoting the signal attenuation and noise level respectively. δ_r and δ_i denote the mmWave noise in the real part and imaginary part respectively, which follow Gaussian distribution for each frequency f: $\delta_r \sim N(\mu_1(f), \sigma_1^2(f))$, $\delta_i \sim N(\mu_2(f), \sigma_2^2(f))$, μ and σ denotes the mean and variance of a normal distribution, respectively.

According to Eq. 1, we generate synthesis training data using clean digital speech samples from the HSC. The digital samples are first transformed into a spectrogram with STFT. Then, in the time-frequency domain, we multiply the transformed spectrogram of digital speech samples with the frequency response of headphone drivers f_d and the acoustic-vibration transformation response of the headphone f_h. For

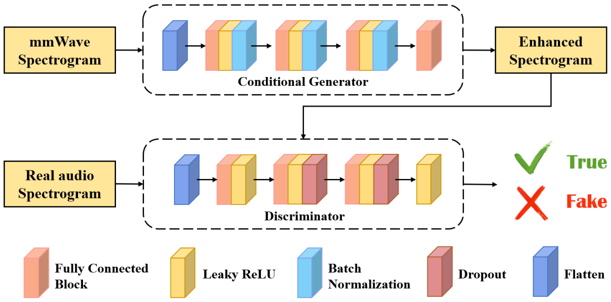

Fig. 11: Structure of cGAN model for speech enhancement.

f_d, we have collected the frequency response information of 47 different headphones from their documentation and randomly select one of them for each generated sample. While for f_h, we determine the responses according to a previous study[27]. After that, we further multiply the damping factor randomly generated from $(0, 1)$ to simulate the signal attenuation. Afterward, the mmWave noises are added. To simulate various SNRs from different setups, we multiply the noise by a normally distributed random number β ranging between 0.1 and 10. Finally, for each frequency component of the current sample, we add noise that follows a normal distribution with different mean and variance for real and imaginary parts.

The synthesis data generated through the aforementioned process is depicted in Fig. 10b. It can be observed that the synthesis data exhibits a high degree of similarity to the mmWave-captured real-world data (Fig. 10c). Through the processes, *mmEar* could generate large-amount synthesis data for pretraining the cGAN model to obtain robustness for various headphones and setups.

B. cGAN Enhancing

The synthesis training data is then utilized to pre-train the cGAN model[22], the architecture of which is shown in Fig. 11. Such an adversary model could be used for detailed information generation[28]. Particularly, this model includes a conditional generator and a discriminator. The generator takes the spectrogram generated from the headphone speech-vibration capturing module as its input and outputs the refined spectrogram. The discriminator takes two kinds of inputs, i.e., a refined spectrogram output by the generator, and the corresponding audio spectrogram, and outputs the discrimination results. With the cGAN structure, the generator and discriminator are trained iteratively, targeting a well-trained generator that could generate high-quality speech spectrograms for eavesdropping.

For the construction details, the generator consists of four fully connected layers with LeakyReLU[29] and Batch Normalization[30] in each layer, while the discriminator consists of three fully connected layers with LeakyReLU and Dropout Normalization[31] with an output rate of 0.4, and it utilizes the sigmoid function[32] as its activation function. The loss of the generator is Mean Square Error (MSE) and the loss of the discriminator is binary cross entropy. The optimizer we use is Adam[33].

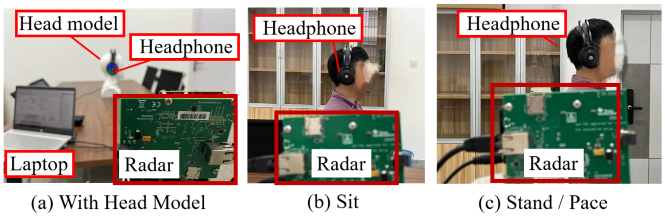

(a) With Head Model (b) Sit (c) Stand / Pace

Fig. 12: Experimental setups of *mmEar*.

The cGAN model is first pre-trained using synthesis data as input. After that, we leverage the real-world mmWave-captured signal to finetune the pre-trained model, further improving the robustness of the model. Finally, we obtain a well-functioned generator model that takes the output spectrogram of *Headphone Speech-vibration Capturing Module* as input and obtains the recovered speech with high quality and intelligibility for eavesdropping.

VII. Evaluation

A. System Setup

The system setup is shown in Fig. 12. We utilize a COTS mmWave radar, Texas Instruments AWR1642BOOST, for transmitting and receiving mmWave signals. The demodulated chirp signals are sampled by the data acquisition board DCA1000EVM and sent to a desktop (HP Pavilion14-ce1004TX) for processing. The cGAN model is implemented using TensorFlow and is trained offline on a desktop NUC with Intel-1260P CPU and 16GB RAM memory. Subsequently, it is deployed on the desktop for real-time speech enhancement. The utilized headphones include HP GH10GS, HP H320GS, Lenovo L7, Sony XM3, ATH-M30x, and earphones include Airpods Pro3 and FreeBuds SE 2. Except for Section. VII-L, the headphones are placed on a human head model as depicted in Fig. 12a. The results are average performance across different headphones and earphones except for Section. VII-I.

B. Dataset and Data Collection

We conduct evaluations using the widely adopted Harvard Speech Repository (HSC)[19] and Open Speech Repository (OSR)[34] datasets. HSC consists 720 sentences spoken by one person while OSR consists sentences from different speakers. To demonstrate *mmEar*'s generalization capability, we select the initial 640 sentences from HSC as training set and sentences from OSR as testing set.

Pre-train Dataset. The pre-train data is generated using the method presented in Section. VI-A. We select the initial 640 sentences in HSC dataset as the digital acoustic samples, and generate 100 samples for each sentence with different generation parameters, forming a dataset with 64000 sentences.

Fine-tune Dataset. The fine-tune data are collected in real-world scenarios. We play the given 640 speech samples from the HSC dataset through the headphones while simultaneously capturing the vibration signals using mmWave radar.

Testing Dataset. In various experimental settings, we collect sentences from the OSR dataset to assess the system's performance.

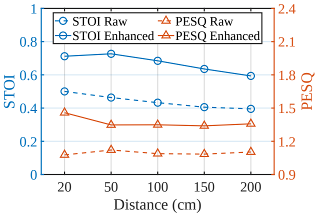

Fig. 13: Impact of attack distance.

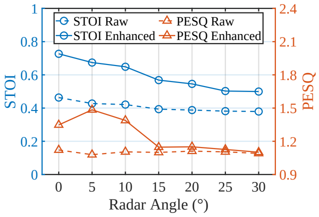

Fig. 14: Impact of incident angle of radar.

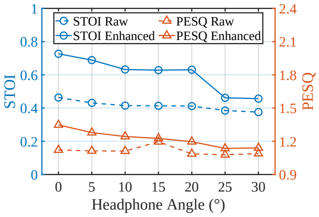

Fig. 15: Impact of incident angle of headphone.

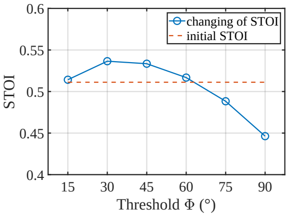

Fig. 16: Impact of threshold Φ.

C. Metrics

Short-Time Objective Intelligibility (STOI): The STOI[23] measures the level of intelligibility of the processed speech by quantifying the similarity between the original speech and processed speech. The STOI value is within [0,1], where higher values indicate better speech intelligibility, an STOI greater than 0.7 generally represents high intelligibility.

Perceptual Evaluation of Speech Quality (PESQ): The PESQ[35] is a quantitative algorithm employed for objectively evaluating the perceived quality of speech signals after conducting transmission or processing. The PESQ is defined in the range of [-0.5,4.5], with increasing values indicating improvement in speech quality.

D. Different Attack Distances

We direct the mmWave radar toward the target headphone and vary the distance between the radar and the headphone from 20cm to 200cm. The result is shown in Fig. 13. Without enhancement, the STOI/PESQ scores of the speech are 0.50/1.08 at a proximity of 20cm, while the enhanced speech achieves scores of 0.71/1.46. Within the range of 20cm to 100cm, showing significant improvements in recovered speech quality and intelligibility.

E. Different Incident Angles of the mmWave Radar

Considering the practical attack scenario where the attacker may not ensure precise alignment of the radar with the headphone, we conduct a controlled experiment to investigate the impact of radar misalignment. The distance between the headphones and the radar is set as 50cm. We vary the radar position to introduce an angle between the radar's line-of-sight and the headphone, ranging from 0° to 30°. The result is presented in Fig. 14. We can observe a general trend that the STOI and PESQ decrease with increasing angle of the mmWave radar. Moreover, the STOI and PESQ remain stable when the radar angle is within 10°, showing a moderate tolerance on mmWave radar angles.

F. Different Incident Angles of Headphones

In a practical eavesdropping scenario, the attackers may not always have the opportunity to transmit mmWave signals perpendicular to the target headphone. Therefore, we also investigate the impact of headphone misalignment. Placing the headphones at a fixed distance of 50cm from the radar, we tilt the headphone body by angles from 0° to 30° to explore their effects on the system's attack performance. The experimental results, shown in Fig. 15, indicate that when the angle is less than 20°, *mmEar* could realize high-quality eavesdropping by significantly improving both STOI and PESQ. This suggests that *mmEar* can still eavesdrop on the speech content played on the headphones even when the headphone body is misaligned to a certain extent.

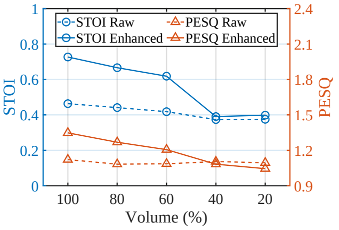

Fig. 17: Impact of different volumes.

G. Impact of threshold Φ of samples

Section. V-B defines a key parameter Φ in our fiant vibration emphasize (FVE) method, which directly influences the quality of captured speech-induced vibrations. We investigated the impact of Φ on the intelligibility of the raw captured vibrations. Concretely, we vary the parameter Φ from 15° to 90° and show the results in Fig. 16. From the figure, it can be observed that when the Φ is set within the range from 30° to 45°, the intelligibility is relatively higher than others, considering the original parameter before FVE is small, the results validate the effectiveness of FVE.

H. Different Volumes of Headphones

We investigated the influence of headphone volume levels by manipulating the volume settings during playback. The headphone volume set at 100%, 80%, 60%, 40%, and 20% of the maximum volume. The result is presented in Fig. 17. It can be observed that when the headphone volume exceeds 60%, the STOI and PESQ for the enhanced audio reach 0.6/1.2. Conversely, when the headphone volume falls below 40%, there is a sharp decline in system performance. This phenomenon arises from the insufficient audio amplitude at lower volume levels, preventing the headphone diaphragm from generating a sufficiently large vibration, thereby impeding the radar's ability to capture meaningful vibrational information.

I. Different Headphones

We conduct experiments with five headphones (HP GH10GS, HP H320GS, Lenovo L7, Sony XM3, ATH-M30x)

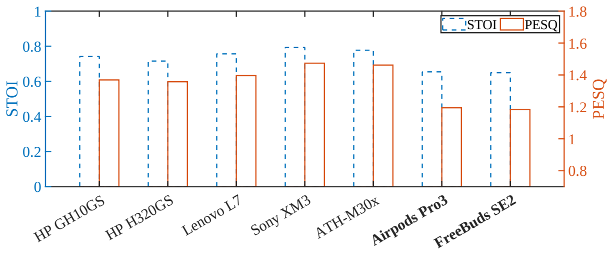

Fig. 18: Different headphones and earphones.

and two earphones (Airpods Pro3 and FreeBuds SE 2), with a distance of 50cm between the headphones/earphones and the radar. The STOI of the different headphones after enhancement is shown in Fig. 18. It indicates that the headphones exhibit higher STOI and PESQ, all-surpassing 0.71/1.35, with Sony XM3 and ATH-M30x over 0.77/1.46. In contrast, earphones demonstrate a slightly lower STOI and PESQ but still exceed 0.64/1.18. This suggests that the system is feasible for both headphones and earphones, but more feasible for headphones that have larger reflection areas.

J. Module Performance

We investigated the impact of the mmEar modules on the system's performance. For each module, we computed metrics for audio processed solely through each module (denoted as *Module 1* and *Module 2*), and through both modules for comparison. The results are depicted in Fig. 19. The experimental findings demonstrate that the audio processed through both *Module 1* and *Module 2* exhibit an STOI improvement of 0.08 compared to audio processed solely through *Module 1* and a 0.06 improvement compared to audio processed solely through *Module 2*. Additionally, the PESQ scores for audio processed through both *Module 1* and *Module 2* are enhanced by 0.24 and 0.21 compared to those processed solely through *Module 1* and solely through *Module 2*, respectively. This indicates that each module of the system significantly influences the final output.

K. Noise Influence

To investigate the impact of background noise on system performance, we conducted experiments under different background white noise environments simulating 50 dB, 60 dB, and 70 dB noise levels, representing quiet office, meeting room, and noisy street scenarios respectively. The distance between the headphone and the radar was set to 50cm with a 0° angle. The experimental results are presented in Fig. 20. From the figure, it can be observed that background noise has minimal effect on the system performance, as both STOI and PESQ values fluctuate around 0.72/1.33.

L. Human Influence

We investigated the impact of various human actions on system performance when wearing headphones. The radar was positioned facing the headphones at a distance of 50cm from the person. As shown in Fig. 12b and Fig. 12c, three different actions of the person were explored, including sitting, standing, and pacing, where sitting and standing involved minimal movement while pacing encompassed moderate movement. The experimental results are illustrated in Fig. 21. From the figure, it can be observed that when the person is sitting and standing, the distance between the person and the radar remains unchanged, and the system still achieves favorable performance, with STOI and PESQ values approximately at 0.66/1.28. However, when the person is pacing, the distance/angle with respect to the headphone and the radar changes, causing a slight decrease in the system performance, but still available to capture speech information.

M. Subjective Scores for Intelligibility.

We recruited 6 volunteers (3 males and 3 females, ages 20-41) to assess the intelligibility of 60 sentences randomly selected from the collected audio under the aforementioned environments, both in their original form (raw) and after enhancement. The volunteers scored intelligibility on a scale of 0 to 10, with higher scores indicating higher speech intelligibility. The average scores given by the 6 volunteers are presented in Fig. 22. In the "sit" and "stand" environments, the raw scores are below 2, showing that most sentences recovered from raw data can not be understood, while the enhanced scores are around 7.2, indicating that a large part of recovered sentences of *mmEar* could be understood by the volunteers. For the "pace" environment, scores for raw vibrations and *mmEar* recovered sentences drop to 0.57/6.5, showing that *mmEar* turns the nearly incomprehensible vibrations into intelligible speech for eavesdropping.

VIII. Related Works

With the surge of mobile computing and Internet-of-things, eavesdropping technology has developed beyond traditional hidden microphones to a broader range of sensors and signals.

A. Eavesdropping with Optical Signals

The laser microphone[2] is a well-known method to eavesdrop with a laser beam, which captures the tiny vibrations of objects induced by sound waves in the victim's room. Similarly, a high-speed camera could also capture sound-induced vibrations and become a visual microphone for eavesdropping[3], so as electro-optical sensors[4] and lidars[5]. Although these optical-based eavesdropping could be launched long distances, they require a static target and a direct path with no occlusion, which limits their scopes.

B. Eavesdropping with Motion Sensors

With the capability to sense vibrations, motion sensors on smartphones are exploited to capture the sound-induced vibrations and perform eavesdropping[6], [7], [8], [9], [10]. Such attack could be achieved with single gyroscope[6] or accelerometer[7], [8], [9], or a combination of multiple motion sensors (accelerometers, gyroscope, and geophone) to realize eavesdropping under limited sampling rates[10]. Besides smartphones, the feasibility of motion sensor-based eavesdropping is proved on VR/AR devices[36], earphones[37], and

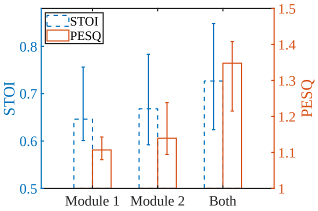

Fig. 19: Impact of modules.

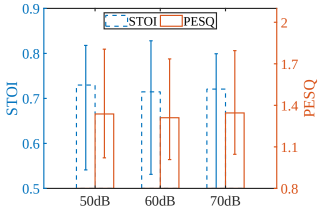

Fig. 20: Impact of noise.

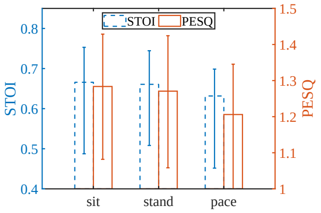

Fig. 21: Impact of human actions.

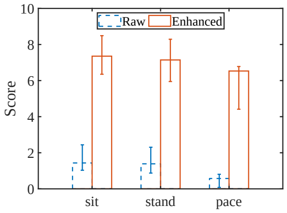

Fig. 22: Subjective scores of human actions.

general IoT devices[38]. However, the assumption of these attacks is the existence of a physical connection between the motion sensor and the sound source, making them not feasible in contactless eavesdropping scenarios.

C. Eavesdropping with RF Signals

Radio frequency (RF) has been explored for contactless eavesdropping in real-world scenarios. As the most widely-deployed RF signal, Wi-Fi shows the feasibility of eavesdropping by leveraging CSI changes[11] and MIMO properties[12] with respect to acoustics, and UWB could achieve better performance with a larger bandwidth[13]. However, these approaches suffer much from multi-path transmission and are thus not robust enough in real-world scenarios. Most recently, the mmWave signal has been exploited for eavesdropping. MILLIEAR[15][39] achieves eavesdropping by extracting phase changes from the reflected mmWave signals targeting the loudspeakers. Along with the path, mmEcho[16] and mmPhone[40] focus on eavesdropping from other objects near the sound source, releasing the requirement of directly targeting the user or the loudspeakers. Meanwhile, mmSpy[17] and mmEve[18] exploit the feasibility of contactless smartphone calls eavesdropping by sensing the speech-induced vibrations on the smartphone's earpiece, showing practical threats in real-world scenarios. However, for the phone call scenarios, people are getting used to wearing headphones or earbuds to prevent privacy leakage, and this work is targeting the more challenging case of headphone eavesdropping with mmWave signals.

D. Other Eavesdropping Approaches

There are other eavesdropping approaches exploiting the side-channel leakage of sound. Motors[41] and hard drives[42] are leveraged for side-channel eavesdropping attacks. Also, magnetic side-channel signals leaked by a microspeaker[43][44] are also utilized for eavesdropping. Different from these methods that require specially designed sensors or scenarios, *mmEar* could launch eavesdropping attacks with COTS mmWave sensors in various real-world scenarios.

IX. Discussion

Defense: The fundamental principle of *mmEar* is to leverage mmWave signals to capture the faint speech-induced vibrations on the headphone surface for eavesdropping. So the defense could be hiding or interfering with the vibration pattern. For the former, more acoustic and vibration-absorbing materials could be added to the headphones to make the vibration weaker than the physical sensing limit of mmWave signals. For the latter, an active vibration signal can be generated by a headphone on its surfaces, which could interfere with the pattern of speech-induced vibrations.

Automatic Speech Recognition: Because the target of *mmEar* is to eavesdrop, The system evaluation is based on scoring the intelligibility of speech using metrics such as STOI and PESQ, as well as human-understanding assessments. We notice that automatic speech recognition (ASR) has already been widely used and intend to involve ASR for more extensive validations in the future.

X. Conclusion

This paper reveals an eavesdropping attack on headphones by capturing the faint speech-induced vibrations on headphone surfaces, and proposes a practical headphone eavesdropping system, *mmEar*, leveraging single COTS mmWave radar. *mmEar* explores the feasibility of mmWave-based speech recovery from extremely faint sound-induced vibrations with a low SNR, and proposes a range of techniques to achieve a robust attack with high generalization ability. Extensive experiments validate the feasibility of the attack, demonstrating the alarming threat of user privacy leakage from widely-used headphones.

Acknowledgments

This research was supported in part by National Natural Science Foundation of China Grant Nos. 62022024, 61972088, 62232004, 62202099, and 62102354, by US National Science Foundation (NSF) Awards 1931871, 1915780, and US Department of Energy (DOE) Award DE-EE0009152, by Jiangsu Provincial Natural Science Foundation of China Grant No. BK20220806, Jiangsu Provincial Key R&D Programs Grant Nos. BE2021729, BE2022680, BE2022065-5, Jiangsu Provincial Key Laboratory of Network and Information Security Grant No. BM2003201, Key Laboratory of Computer Network and Information Integration of Ministry of Education of China Grant No. 93K-9, and Collaborative Innovation Center of Novel Software Technology and Industrialization. Any opinions, findings, conclusions, and recommendations in this paper are those of the authors and do not necessarily reflect the views of the funding agencies.

References

[1] G. V. RESERACH, "Earphones and headphones market size, share & trends analysis report. [online]. avaliable:," 2023. [Online]. Available: https://www.grandviewresearch.com/industry-analysis/earphone-and-headphone-market/toc

[2] R. P. Muscatell, "Laser microphone," The Journal of the Acoustical Society of America, vol. 76, no. 4, pp. 1284–1284, 1984.

[3] A. Davis, M. Rubinstein, N. Wadhwa, G. J. Mysore, F. Durand, and W. T. Freeman, "The visual microphone: Passive recovery of sound from video," ACM Trans. Graph., vol. 33, no. 4, jul 2014.

[4] B. Nassi, Y. Pirutin, R. Swisa, A. Shamir, Y. Elovici, and B. Zadov, "Lamphone: Passive sound recovery from a desk lamp's light bulb vibrations," in Proc. USENIX Security'22. USENIX Association, 2022, pp. 4401–4417.

[5] S. Sami, Y. Dai, S. R. X. Tan, N. Roy, and J. Han, "Spying with your robot vacuum cleaner: Eavesdropping via lidar sensors," in Proc. SenSys'20. ACM, 2020, pp. 354–367.

[6] Y. Michalevsky, D. Boneh, and G. Nakibly, "Gyrophone: Recognizing speech from gyroscope signals," in Proc. USENIX Security'14. USENIX Association, 2014, pp. 1053–1067.

[7] S. A. Anand and N. Saxena, "Speechless: Analyzing the threat to speech privacy from smartphone motion sensors," in 2018 IEEE Symposium on Security and Privacy (SP). IEEE, 2018, pp. 1000–1017.

[8] S. A. Anand, C. Wang, J. Liu, N. Saxena, and Y. Chen, "Spearphone: A lightweight speech privacy exploit via accelerometer-sensed reverberations from smartphone loudspeakers," in Proc. WiSec'21. ACM, 2021, pp. 288–299.

[9] Z. Ba, T. Zheng, X. Zhang, Z. Qin, B. Li, X. Liu, and K. Ren, "Learning-based practical smartphone eavesdropping with built-in accelerometer." in Proc. NDSS'20, vol. 2020, 2020, pp. 1–18.

[10] Y. Liang, Y. Qin, Q. Li, X. Yan, L. Huangfu, S. Samtani, B. Guo, and Z. Yu, "An escalated eavesdropping attack on mobile devices via low-resolution vibration signals," IEEE Transactions on Dependable and Secure Computing, vol. 20, no. 4, pp. 3037–3050, 2023.

[11] G. Wang, Y. Zou, Z. Zhou, K. Wu, and L. M. Ni, "We can hear you with wi-fi!" IEEE Transactions on Mobile Computing, vol. 15, no. 11, pp. 2907–2920, 2016.

[12] T. Wei, S. Wang, A. Zhou, and X. Zhang, "Acoustic eavesdropping through wireless vibrometry," in Proc. MobiCom'15. ACM, 2015, pp. 130–141.

[13] Z. Wang, Z. Chen, A. D. Singh, L. Garcia, J. Luo, and M. B. Srivastava, "Uwhear: Through-wall extraction and separation of audio vibrations using wireless signals," in Proc. SenSys'20. ACM, 2020, pp. 1–14.

[14] X. Xu, J. Yu, C. Ma, Y. Ren, H. Liu, Y. Zhu, Y.-C. Chen, and F. Tang, "mmecg: Monitoring human cardiac cycle in driving environments leveraging millimeter wave," in Proc. INFOCOM'22. IEEE, 2022, pp. 90–99.

[15] P. Hu, Y. Ma, P. S. Santhalingam, P. H. Pathak, and X. Cheng, "Milliear: Millimeter-wave acoustic eavesdropping with unconstrained vocabulary," in Proc. IEEE INFOCOM'22. IEEE, 2022, pp. 11–20.

[16] P. Hu, W. Li, R. Spolaor, and X. Cheng, "mmecho: A mmwave-based acoustic eavesdropping method," in IEEE Symposium on Security and Privacy (SP). IEEE, 2023, pp. 1840–1856.

[17] S. Basak and M. Gowda, "mmspy: Spying phone calls using mmwave radars," in 2022 IEEE Symposium on Security and Privacy (SP). IEEE, 2022, pp. 1211–1228.

[18] C. Wang, F. Lin, T. Liu, K. Zheng, Z. Wang, Z. Li, M.-C. Huang, W. Xu, and K. Ren, "mmeve: Eavesdropping on smartphone's earpiece via cots mmwave device," in Proc. MobiCom'22. ACM, 2022, pp. 338–351.

[19] P. Demonte, "Harvard speech corpus–audio recording 2019," University of Salford Collection, 2019.

[20] I. Mikhelson, S. Bakhtiari, T. W. Elmer, and A. V. Sahakian, "Remote sensing of heart rate and patterns of respiration on a stationary subject using 94-ghz millimeter-wave interferometry," IEEE Trans. Biomed. Eng., vol. 58, no. 6, pp. 1671–1677, 2011.

[21] C. Jiang, J. Guo, Y. He, M. Jin, S. Li, and Y. Liu, "mmvib: micrometer-level vibration measurement with mmwave radar," in Proc. MoboCom'20. ACM, 2020, pp. 1–13.

[22] M. Mirza and S. Osindero, "Conditional generative adversarial nets," arXiv preprint arXiv:1411.1784, 2014.

[23] C. H. Taal, R. C. Hendriks, R. Heusdens, and J. Jensen, "An algorithm for intelligibility prediction of time–frequency weighted noisy speech," IEEE Transactions on Audio, Speech, and Language Processing, vol. 19, no. 7, pp. 2125–2136, 2011.

[24] Y. Xu, J. Du, L.-R. Dai, and C.-H. Lee, "A regression approach to speech enhancement based on deep neural networks," IEEE/ACM Transactions on Audio, Speech, and Language Processing, vol. 23, no. 1, pp. 7–19, 2015.

[25] K. AN, "Sulla determinazione empirica di una legge didistribuzione," Giorn Dell'inst Ital Degli Att, vol. 4, pp. 89–91, 1933.

[26] N. V. Smirnov, "Approximate laws of distribution of random variables from empirical data," Uspekhi Matematicheskikh Nauk, no. 10, pp. 179–206, 1944.

[27] K. Carillo, F. Sgard, and O. Doutres, "Numerical study of the broadband vibro-acoustic response of an earmuff," Applied Acoustics, vol. 134, pp. 25–33, 2018.

[28] X. Xu, J. Yu, Y. Chen, Y. Zhu, L. Kong, and M. Li, "Breathlistener: Fine-grained breathing monitoring in driving environments utilizing acoustic signals," in Proc. MobiSys'19. ACM, 2019, pp. 54–66.

[29] A. L. Maas, A. Y. Hannun, and A. Y. Ng, "Rectifier nonlinearities improve neural network acoustic models," in Proc. ICASSP'13. IEEE, 2013, pp. 1234–1238.

[30] S. Ioffe and C. Szegedy, "Batch normalization: Accelerating deep network training by reducing internal covariate shift," in Proc. ICML'15. JMLR.org, 2015, pp. 448–456.

[31] N. Srivastava, G. Hinton, A. Krizhevsky, I. Sutskever, and R. Salakhutdinov, "Dropout: a simple way to prevent neural networks from overfitting," The journal of machine learning research, vol. 15, no. 1, pp. 1929–1958, 2014.

[32] W. S. McCulloch and W. Pitts, "A logical calculus of the ideas immanent in nervous activity," The bulletin of mathematical biophysics, vol. 5, pp. 115–133, 1943.

[33] D. P. Kingma and J. Ba, "Adam: A method for stochastic optimization," arXiv preprint arXiv:1412.6980, 2014.

[34] V. Troubleshooter, "The open speech repository," 2010.

[35] A. W. Rix, J. G. Beerends, M. P. Hollier, and A. P. Hekstra, "Perceptual evaluation of speech quality (pesq)-a new method for speech quality assessment of telephone networks and codecs," in IEEE international conference on acoustics, speech, and signal processing, vol. 2. IEEE, 2001, pp. 749–752.

[36] C. Shi, X. Xu, T. Zhang, P. Walker, Y. Wu, J. Liu, N. Saxena, Y. Chen, and J. Yu, "Face-mic: Inferring live speech and speaker identity via subtle facial dynamics captured by ar/vr motion sensors," in Proc. MobiCom'21. ACM, 2021, pp. 478–490.

[37] Y. Cao, F. Li, H. Chen, X. Liu, C. Duan, and Y. Wang, "I can hear you without a microphone: Live speech eavesdropping from earphone motion sensors," in Proc. INFOCOM'23. IEEE, 2023, pp. 1–10.

[38] J. Han, A. J. Chung, and P. Tague, "Pitchln: Eavesdropping via intelligible speech reconstruction using non-acoustic sensor fusion," in Proc. IPSN'17. ACM, 2017, pp. 181–192.

[39] P. Hu, W. Li, Y. Ma, P. S. Santhalingam, P. Pathak, H. Li, H. Zhang, G. Zhang, X. Cheng, and P. Mohapatra, "Towards unconstrained vocabulary eavesdropping with mmwave radar using gan," IEEE Transactions on Mobile Computing, 2022.

[40] C. Wang, F. Lin, T. Liu, Z. Liu, Y. Shen, Z. Ba, L. Lu, W. Xu, and K. Ren, "mmphone: Acoustic eavesdropping on loudspeakers via mmwave-characterized piezoelectric effect," in Proc. IEEE INFOCOM'22. IEEE, 2022, pp. 820–829.

[41] N. Roy and R. Roy Choudhury, "Listening through a vibration motor," in Proc. MobiSys'16. ACM, 2016, pp. 57–69.

[42] A. Kwong, W. Xu, and K. Fu, "Hard drive of hearing: Disks that eavesdrop with a synthesized microphone," in IEEE symposium on security and privacy (SP). IEEE, 2019, pp. 905–919.

[43] J. Choi, H.-Y. Yang, and D.-H. Cho, "Tempest comeback: A realistic audio eavesdropping threat on mixed-signal socs," in Proc. CCS'20. ACM, 2020, pp. 1085–1101.

[44] Q. Liao, Y. Huang, Y. Huang, Y. Zhong, H. Jin, and K. Wu, "Magear: Eavesdropping via audio recovery using magnetic side channel," in Proc. MobiSys'22. ACM, 2022, pp. 371–383.